A NEW DISCRETE SIMULATION METHOD FOR MODELING CHAR GASIFICATION IN THE DIFFUSION-CONTROLLED REGIME

Kyriacos Zygourakis
Department of Chemical Engineering
Rice University
Houston, TX 77251-1892

ABSTRACT

Cellular automata and discrete iterations are employed to develop a new simulation method for gas-solid reactions. This approach overcomes many of the limitations of earlier models since it can handle heterogeneous systems with multiple porous reactants and arbitrary pore/solid geometries. The new models are used to simulate the gasification of porous char particles under conditions leading to strong intraparticle diffusional limitations and to low utilization of the micropores. In order to accurately account for the effects of the macropore structure on char reactivity, the new models employ computational grids obtained by digitizing images of actual char particle cross-sections using an optical microscope equipped with a video camera and an image processing computer. Simulation results are presented from multiple runs performed on several char samples that were prepared in our laboratory by pyrolyzing two parent coals under various operating conditions. Model predictions are compared and analyzed in order to elucidate the effects of the macropore structure on the gasification rates and particle burn-out times.

MODEL DEVELOPMENT

This study will consider a porous solid that reacts with one or more gaseous reactants to produce one or more gaseous products. Thus, the developed model can be applied to all the important coal gasification and combustion reactions.

Discrete models employ rectangular arrays of usually square cells to simulate the temporal evolution of pore structures in reacting systems. Our earlier discrete models (Sandmann and Zygourakis, 1986) defined the pores of a solid reactant (char) by randomly distributing on the grid overlapping *regular geometrical entities* (circles, spheres or cylinders) of a given size distribution. Direct microscopic measurements, however, revealed that char particles exhibit highly irregular pore structures (Zygourakis and Glass, 1988; Zygourakis, 1988).

Cellular Arrays and Reaction Rules

A new discrete simulation approach was developed to overcome the computational complexities introduced when considering heterogeneous reactions in system with arbitrary pore/solid geometries and multiple porous reactants. The new approach is based on ***cellular automata*** and ***discrete iterations***. The evolving pore structure of multicomponent systems is again modeled on rectangular arrays of cells. Each cell can exist in one of several possible states. It can represent, for example, a small volume element of either solid reactant, a pore that is accessible to the gaseous reactants etc.

The important thing to notice about our simulations approach is that the initial configurations of the cellular arrays are obtained ***directly from the digitized images of actual char particle cross-sections***. For example, Fig. 1A is a 1024x1040 binary image of a char particle cross-section. Black pixels correspond to the char matrix, while the particle exterior and the interior macropores are denoted by white.

The number of possible states for each cell depends on the assumed reaction

regime. This study will consider the following two limiting cases of reaction regimes.

Regime A: When there are no diffusional limitations in the macropores, the entire surface area associated with the macropores is available for reaction. Then each cell of our computational grid can exist in one of two possible states: it can represent a small volume element of either solid reactant or pore void. An initial computational grid for this regime is shown in Fig. 1A. The evolution of the pore structure is modeled by updating the initial cellular array at equally spaced time instants $t^1, t^2, \ldots, t^r, t^{r+1}, \ldots$ as follows: *If at time t^r a solid reactant (black) cell is adjacent to one or more gaseous reactant (white) cells, then this solid cell may be changed to a pore void cell or* ***reacted*** at the next *time level $t^{r+1} = t^r + \Delta t$*. The solid cells are reacted according to a probabilistic algorithm that guarantees isotropic consumption of the solid reactant. This algorithm erodes a single layer of pixels from the entire surface area exposed to gaseous reactants during each iteration step Δt. Figs. 1B and 1C show the computational grid of Fig. 1A after 10 and 16 iteration steps that correspond to solid conversions of 24.9% and 38.4%. Fig. 1D shows the temporal evolution of the predicted reaction rate as a function of the number of iterations.

Regime B: In this regime, only the surface area directly accessible to reactants from the irregular particle exterior participates in the reaction. Internal macropores are not initially accessible to the gaseous reactants. When the reaction front "opens" these interior pores, however, their surface area becomes available for reaction. These rules are implemented by allowing each cell of the computational grid to exist in one of three possible states (see Fig. 2A): it can be a solid reactant cell (black), a cell occupied by gaseous reactants or "open pore cell" (white) or a cell belonging to a "closed macropore" (grey). The initial cellular array is updated according to the following rules: ***(1)*** A solid reactant (black) cell may "react" (changing its state to white), if its immediate neighborhood contains one or more gaseous reactant (white) cells; ***(2)*** A solid reactant (black) cell will not change its state, if it is surrounded only by solid (black) or "closed pore" (grey) cells; ***(3)*** If "closed pore" (grey) cells get exposed to gaseous reactant (white) cells, their state may change to gaseous reactant (white). Figs. 2B and 2C show the configuration of the cellular array at two different iteration steps and Fig. 2D again shows the evolution of the predicted reaction rate. In general, gaseous reactant cells "consume" solid or closed pore cells at different rates. These rates can be appropriately adjusted to account for different degrees of diffusional limitations in the macropores opening up for reaction.

Estimating Reaction Rates from Discrete Simulations

The simulation results can be related to experimental gasification data as follows. If m(t) is the mass of solid remaining at time t, the specific rate R_m of the heterogeneous reaction can be expressed as

$$R_m \equiv \frac{1}{m(t)} \frac{dm}{dt} = S_g(X)\ \mathfrak{R}_s(c,T;a) \tag{1}$$

where S_g is the ***specific pore surface area available for reaction*** (expressed in m^2 of surface area per kg of solid), $\mathfrak{R}_s(c,T;a)$ is the intrinsic reaction rate expressed in (kg of solid)/(s)(m^2 of surface area), c denotes the gaseous reactant concentrations, T is the temperature and a(X) is a measure of the surface activity. Since the porous solid is consumed during the reaction, the surface area S_g changes drastically with the solid conversion X defined by

$$X = \frac{m_o - m(t)}{m_o} \tag{2}$$

where m_o is the mass of the unreacted solid. Intraparticle diffusional limitations are accounted by Eq. (2), since such limitations (in the micropores, for

example) may dramatically decrease the total surface area S_g available for reaction.

Let dV be the volume of solid consumed by the heterogeneous reaction over a time period equal to dt. Then

$$\rho_s \frac{dV}{dt} = m(t)\ S_g\ \Re_s(c,T;a) \tag{3}$$

where ρ_s is the density of the solid reactant. If the reaction rate is uniform over the entire surface area S_g, a layer of solid with uniform thickness dz will be consumed over the time period dt. Thus, $dV = S_g\ m(t)\ dz$ and Eq. (3) becomes

$$\frac{dz}{dt} = \frac{\Re_s(c,T;a)}{\rho_s} \tag{4}$$

The previous equations can be used to normalize the reaction rates predicted by the discrete models. At every simulation step, we erode a single layer of pixels from the solid surface area available for reaction. Thus, every erosion step corresponds to a time interval Δt that equals the time required to convert a solid layer of uniform thickness Δz, where Δz is the pixel size. From Eq. (4)

$$\frac{\Delta z}{\Delta t} \approx \frac{\Re_s(c,T;a)}{\rho_s} \tag{5}$$

and if two simulations are carried out on images with different pixel sizes Δz and Δz^*, their time steps will be related according to the formula

$$\frac{\Delta z}{\Delta t} = \frac{\Delta z^*}{\Delta t^*} \tag{6}$$

The measured reaction rates are most often normalized with respect to the mass m_o of the unreacted solid or

$$R_o \equiv \frac{1}{m_o}\frac{dm}{dt} = (1-X)\ R_m \tag{7}$$

Let now N_o be the number of solid reactant pixels on the initial computational grid and let $(\Delta N)^r$ be the number of solid pixels that react in the time interval $[t^r, t^{r+1}]$. The specific rate R_o^r for this step can be computed as

$$R_o^r\ \Delta t = \frac{(\Delta N)^r}{N_o} \tag{8}$$

Let Δz be the pixel size (in μm) for this image and let Δt^* be the time required to react a layer of solid with uniform thickness equal to $\Delta z^* = 1$ μm. Eqs. (8) and (6) yield

$$R_o^r\ \Delta t^* = \frac{(\Delta N)^r}{N_o}\ \frac{\Delta z^*}{\Delta z} \tag{9}$$

Thus, Eq. (9) provides specific reaction rates that are independent of the pixel size of the digitized images used in the simulations.

Using Eq. (5), the value of Δt^* can be computed from the value of the intrinsic rate $\Re_s(c,T;a)$ at the appropriate conditions. Most often, however, the reactivity data obtained at various temperatures and reactant concentrations are normalized so as to obtain **master curves** that yield (within experimental error) the dependence of the active surface area on conversion. Such master curves can be obtained directly from the simulations by plotting the dimensionless rate $R_e^r \equiv R_o^r\ \Delta t^*$ vs. either the conversion or a dimensionless time θ where

$$\theta = \frac{t}{\Delta t^*} \approx \frac{t\ \Re_s(c,T;a)}{\Delta z^*\ \rho_s} \tag{10}$$

The predictions of observed reaction rates assume, of course, that the surface activity and the intrinsic reaction rate $\Re_s$ do not change appreciably with conversion. Since several simulations are performed for each char sample, the

average rate R_e^r is computed by the formula

$$R_e^r = \frac{\sum (\Delta N)^r}{\sum N_o} \frac{\Delta x^*}{\Delta x} \tag{11}$$

where the summations are taken over all simulation runs performed for different particle cross-sections from the same char sample. The reaction rates computed according to Eq. (11) can be directly compared regardless of the amount of solid in each sample or the magnification used when acquiring the digitized images.

The simulations described here are performed on two-dimensional cellular arrays that are discrete approximations of cross-sections of actual char particles. At each iteration step, heterogeneous reactions occur at the boundaries (perimeter) of the two-dimensional pore profiles (see Figs. 1 and 2). Results from ***two-dimensional simulations***, however, can be used to obtain accurate ***estimates*** of reaction rates occurring on our ***three-dimensional structures***. If we assume that the cross-sections used for our simulations form a "random plane section" through our population of char particles, unbiased estimators of the macroporosity ε and of the macropore surface density S_v (in (cm^2 pore surface)/(cm^3 particle)) are given (Weibel, 1980) by

$$\varepsilon = \frac{A_a}{A_c} \qquad S_v = \frac{1}{4\pi} \frac{B_a}{A_c} \tag{12}$$

where A_a is the total area of pore profiles, B_a is the total pore profile boundary length and A_c is the total area of particle cross-sections. Note that S_v can be estimated from two-dimensional sections ***without any restricting assumptions concerning the geometrical shape of the pores*** (DeHoff, 1983). The three primary quantities A_a, A_c and B_a can be easily obtained from the particle cross-sections via image processing techniques, and the total specific macropore surface area S_t (expressed in m^2 per kg of solid) can be easily computed as

$$S_t = \frac{S_v}{(1-\varepsilon)\ \rho_s} \tag{14}$$

When reaction takes place in Regime A, there are no diffusional limitations in the macropores and the entire macropore surface area reacts at the same rate ($S_g = S_t$). If we assume that the evolving cross-sections continue to constitute "random sections" for our char particle population, the discrete simulations provide accurate ***estimates*** of the changing surface area of the ***three-dimensional macropores*** and, consequently, of the temporal evolution of reaction rates in Regime A (see Eqs. 1 or 7). Although these arguments do not hold in the general case of reaction in Regime B (where the internal macropores are assumed to be "closed" and $S_g \neq S_t$), approximate estimates of reaction rates can be obtained if we assume that the internal pores for any cross-section do not become available for reaction due to burn-through occurring at planes above or below the studied one. Although this assumption can be easily relaxed in our discrete models, such an extension of the models would require information about the connectivity of the three-dimensional macropores. Such structural information is not currently available.

RESULTS AND DISCUSSION

An earlier study (Zygourakis, 1988) presented the results from microscopic investigations on the macropore structure of coal chars prepared under different pyrolysis conditions. Char particles collected from several runs at each set of conditions were embedded in an epoxy-resin block, and one side of the block was polished to reveal random cross-sections. Digitized images of particle cross-sections were then acquired and segmented on an image processing computer to identify the char matrix and macropores with diameter greater than 1 μm.

The original binary images had a resolution of 640x480 pixels. Many char samples, however, exhibited macropores with very thin walls that were consumed in only a few iterations. In order to increase the accuracy of the simulations, each 640x480 image was first magnified by a factor of 4. The magnified 2560x1920 images were smoothed to remove the edge "jaggedness" that is introduced by simple magnification operations. Several runs were also carried out by magnifying the original images by a factor of 8 and smoothing them. Results obtained from simulations with 5120x3840 images showed only small differences from those obtained from simulations with 2560x1920 images. For each char sample, 48 runs were performed with different particle cross-sections and the results were averaged as previously discussed.

We simulated first a gas-solid reaction taking place in Regime A, where there are no diffusional limitations in the macropores and the entire macropore surface area reacts at the same rate. Fig. 3 presents the reactivity patterns predicted for 4 chars produced from an Illinois #6 coal at different pyrolysis heating rates. The model predictions reflect the wide differences in the pore structure of these chars (Zygourakis, 1988). All chars exhibit an initial increase in reactivity caused by macropore growth. Such a behavior cannot be predicted by shrinking-core models. Since the chars produced at high heating rates (10 and 1000 °C/s) have almost exclusively large thin-walled cavities (ibid.), the predicted rates drop dramatically when the thin walls separating the macropores are consumed. The rate vs. conversion patterns exhibit a small maximum that is shifted towards higher conversion levels for the chars produced at high heating rates. Fig. 4 shows the predicted reactivity behavior for three chars produced from different size fractions of Illinois #6 coal particles at a pyrolysis heating rate of 10 °C/s. Small coal particle sizes lead to chars with larger macropore surface areas and, hence, with higher reactivity. These high reaction rates fall rapidly, however, and the maximum in the rate vs. conversion pattern shifts towards lower conversions. Fig. 5 shows the predicted reactivity behavior for two chars produced from a lignite coal at 0.1 and 1000 °C/s. Small differences in char reactivity can be seen from these graphs, an observation consistent with the pyrolysis mechanism and the pore structure of these chars.

Fig. 6 presents simulation results obtained when 4 Illinois #6 chars (see Fig. 3) react in Regime B, where the internal macropores are not initially accessible to the gaseous reactants. Due to the progressive opening of internal macropores, the reactivity of chars produced at low pyrolysis heating rates (e.g. 0.1 °C/s) remains high even at fairly large values of conversion. The reactivity patterns of chars produced at high pyrolysis rates (e.g. 1000 °C/s) show several local maxima that correspond to the opening up of internal large macropores and of the smaller secondary vesicles formed in the walls separating the larger macropores (see Zygourakis, 1988). Such jumps in the reaction rate have been observed during single-particle gasification experiments (Sundback et. al., 1984).

ACKNOWLEDGMENT

This work was partially supported by the Department of Energy under the contract DE-FG22-87PC79930.

REFERENCES

DeHoff, R.T., *J. Microscopy*, ***131***, 259 (1983).
Sandmann, C.W. and Zygourakis, K., *Chem. Eng. Sci.*, ***41***, 733 (1986).
Sundback, C.A., Beer, J.M. and Sarofim, A.F., *Procs. 20th International Symposium on Combustion*, p. 1495, Ann Arbor, Michigan, August 12-17 (1984).
Weibel, E.R., *Stereological Methods*, vol. ***2***, Academic Press (1980).
Zygourakis, K. and Glass, M.W., *Chem. Eng. Commun.*, ***70***, 39 (1988).
Zygourakis, K., *ACS Div. Fuel Chem. Preprints*, ***33(4)***, 951 (1988).

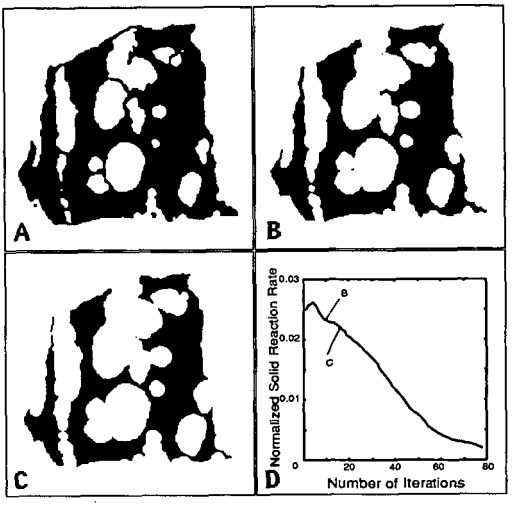

Figure 1: Binary images showing the computational grids at three conversion levels (A: X=0.00, B: X=24.9%, C: X=38.4%) and the evolution of normalized reaction rates for a simulation in reaction Regime A (two-state computational cells).

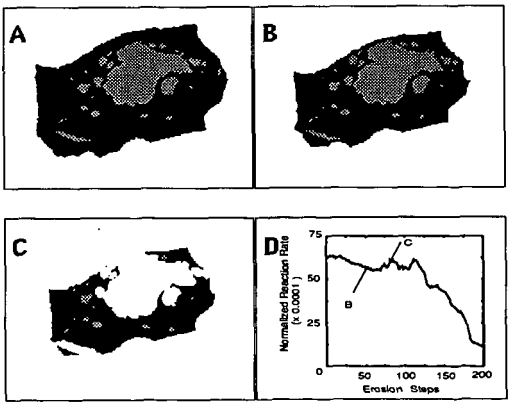

Figure 2: Binary images showing the computational grids at three conversion levels (A: X=0.00, B: X=30.9%, C: X=49.1%) and the evolution of normalized reaction rates for a simulation in reaction Regime B (three-state computational cells).

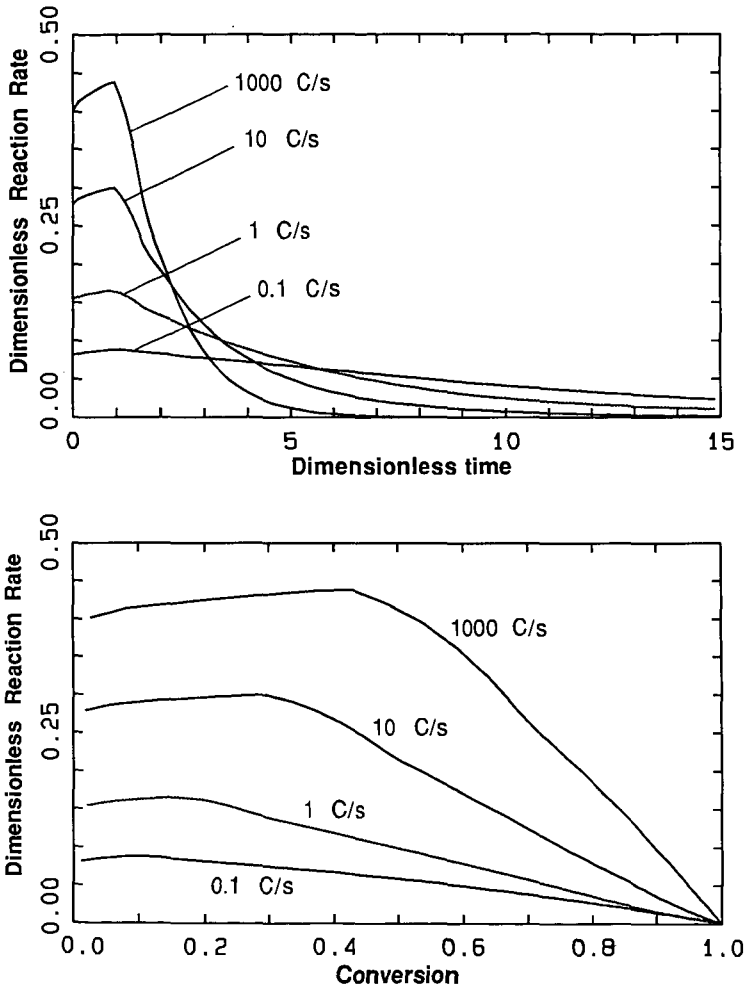

Figure 3: Reactivity patterns predicted for reaction in Regime A of four Illinois #6 chars produced at different pyrolysis heating rates (Coal particle size: 50-60 mesh). Each curve is the average computed from 48 runs with different particle cross-sections.

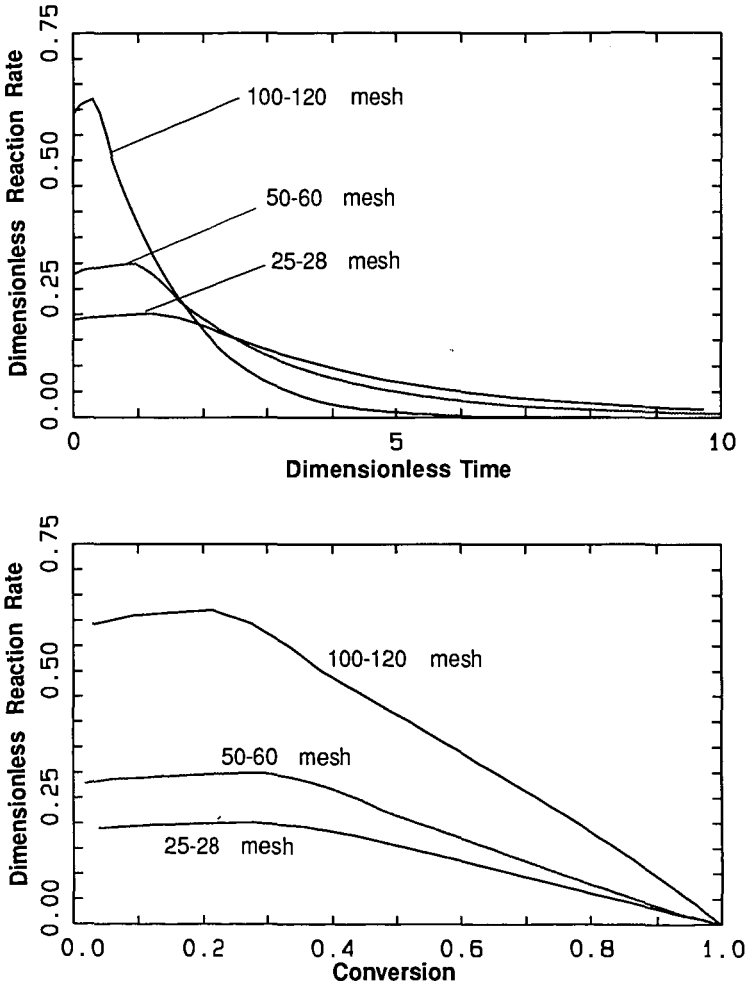

Figure 4: Reactivity patterns predicted for reaction in Regime A of three Illinois #6 chars produced from different coal particle size fractions (Pyrolysis heating rate: 10 °C/s). Each curve is the average computed from 48 runs with different particle cross-sections.

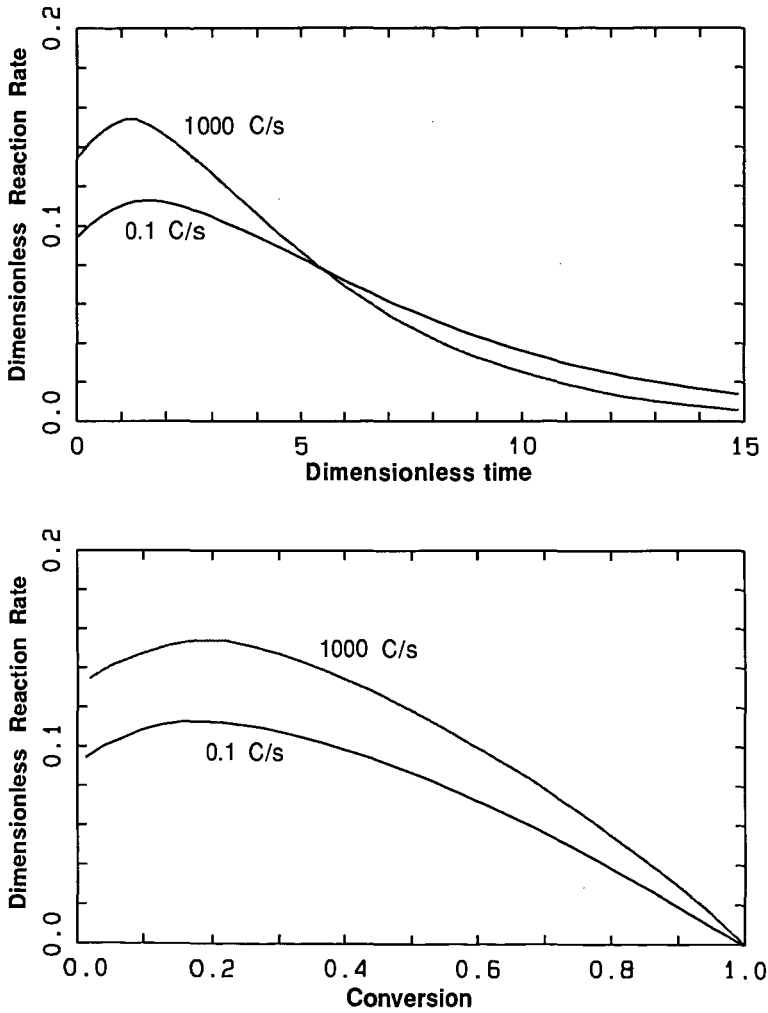

Figure 5: Reactivity patterns predicted for reaction in Regime A of two lignite chars produced at different pyrolysis heating rates (Coal particle size: 50-60 mesh). Each curve is the average computed from 48 runs with different particle cross-sections.

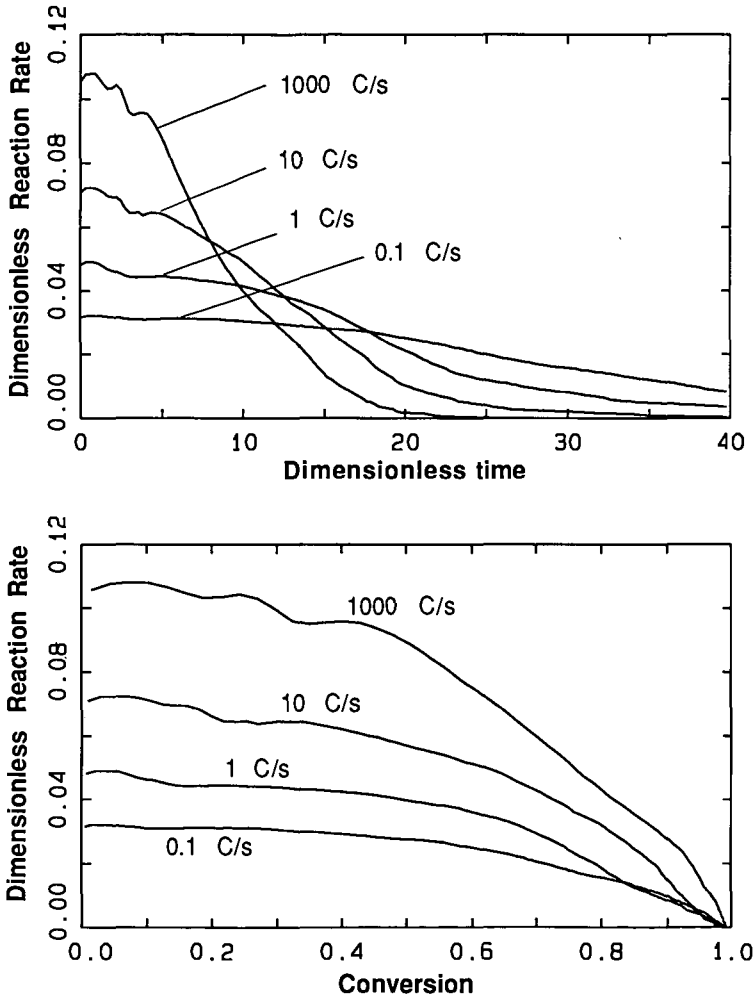

Figure 6: Reactivity patterns predicted for reaction in Regime B of four Illinois #6 chars produced at different pyrolysis heating rates (Coal particle size: 50-60 mesh). Each curve is the average computed from 48 runs with different particle cross-sections.